Measurement of monoenergetic neutrons from the $\overline{pd}$ reaction at rest

M. Chiba,[7] K. Doi,[6] T. Fujitani,[6] K. Inoue,[5] J. Iwahori,[1,*] M. Kawaguti,[1,†] M. Kobayashi,[3] M. Koike,[2] T. Kozuki,[6] S. Kurokawa,[3] H. Kusumoto,[6,‡] H. Nagano,[6] Y. Nagashima,[6] T. Omori,[6,§] S. Sugimoto,[6,‖] M. Takasaki,[3] F. Takeutchi,[4] M. Tsuchiya,[6] M. Ueda,[6] Y. Yamaguchi,[6] and H. Yoshida[1,¶]
(Fukui-INS-KEK-Kyoto Sangyo-Meisei-Osaka-Tokyo Metropolitan Collaboration)

[1]*Faculty of Engineering, Fukui University, Fukui 910, Japan*
[2]*Institute for Nuclear Study, University of Tokyo, Tanashi, Tokyo 138, Japan*
[3]*National Laboratory for High Energy Physics (KEK), Tsukiba 305, Japan*
[4]*Faculty of Science, Kyoto Sangyo University, Kitaku, Kyoto 603, Japan*
[5]*Faculty of Science and Technology, Meisei University, Hino 191, Japan*
[6]*Physics Department, Osaka University, Toyonaka, Osaka 560, Japan*
[7]*Physics Department, Tokyo Metropolitan University, Hachioji 192-03, Japan*
(Received 15 July 1996)

To search for baryonium states, a highly sensitive experiment with good statistics has been carried out at KEK by using an antiproton beam, deuterium target, and time-of-flight counter together with a modularized NaI(Tl) detector. At the 4σ level, no narrow peaks due to the production of baryonia in the $\overline{pd}\rightarrow Bn$ reaction have been observed in the neutron spectra. At lower significance levels, however, we have observed four narrow peaks with $3.7\sigma-3.5\sigma$, and two at an even lower significance level, in different charge-multiplicity final states. The recoil momentum distribution of the neutrons has been extracted for the channel with zero charge prongs. The energy spectra for γ rays in coincidence with the neutron have been also obtained. [S0556-2821(97)03901-5]

PACS number(s): 13.75.Cs, 14.20.Gk, 14.40.Cs, 21.10.Dr

I. INTRODUCTION

Baryonia, diquark-antidiquark bound states, have been extensively sought for more than a decade. Their existence is theoretically predicted both in the quark model and in the nuclear potential model (see the references in [1,2]). The baryons below the $\overline{NN}$ threshold are expected to have surprisingly long lives. The existence of such states below the threshold was first reported by Gray *et al.* in 1971 in an experiment at BNL using $\overline{p}$ stopped in the deuterium bubble chamber [3]. An enhancement of 5σ has been found in the mass distribution of four and six pion system, indicating the existence of a negatively charged baryonium of 1795 MeV/c^2. Since then, to study these states, many experiments have been carried out, especially in the $\overline{pp}\rightarrow B^0\gamma$ reaction channel associated with emission of a monochromatic γ ray, since the measurement of the γ-ray energy with high precision is relatively easy.

Kalogeropoulos *et al.*, however, failed to see a baryonium state in a bubble chamber experiment at BNL in the mass range between 1670 and 1820 MeV/c^2 [4], but then, in an experiment at the CERN Proton Synchrotron, Pavlopoulos *et al.* have observed three monochromatic lines in the inclusive γ-ray spectrum from $\overline{p}$ stopped in the hydrogen target [5]. The yields were $(1-3)\times10^{-3}$ per annihilation and the statistical significance was 2 to 3σ. Later, two of these levels (1684 and 1646 MeV/c^2) have been confirmed, and two more states (1771 and 1210 MeV/c^2) have been newly found by the same group at CERN with the use of an improved γ detection system with 54 pieces of modular NaI crystals [6]. Brando *et al.* also confirmed at BNL the 1771 MeV/c^2 state [7] using a magnetic pair spectrometer for the γ measurement.

Ever since, however, these levels have not been confirmed in the $\overline{pp}\rightarrow B^0\gamma$ reaction channel in experiments with higher sensitivity. We carried out also an experiment with a good statistics at KEK [1,8]. The result was negative, and a 4σ upper limit of $(1.2-0.2)\times10^{-3}$ per stopped $\overline{p}$ in the mass range of 1040 to 1795 MeV/c^2 has been obtained. Two experiments at the CERN Low Energy Antiproton Ring (LEAR), one using BGO crystals [9], and the other using magnetic pair spectrometer [2,10], have been performed, and they both gave negative results too.

However, the possibility of the observation of baryonia depends on the production process looked at. It is worthwhile to investigate also the $\overline{pp}\rightarrow B\pi$ strong interaction process, because its yield per annihilation can be larger, and it can selectively populate $I=1$ baryonium states. Bertini *et al.* measured the π^- spectrum from the $\overline{pp}\rightarrow B^+\pi^-$ reaction using 1.3 GeV/c $\overline{p}$ and failed to see narrow states [11]. Later two experiments at CERN with higher precision, one using magnetic spectrometer [12], and the other using a gaseous

*Present address: Kochi Medical School, Nankoku, Kochi, 783 Japan.
†Deceased.
‡Present address: Dept. Environm. Info., Keio University, Fujisawa, 252 Japan.
§Present address: KEK, National Laboratory for High Energy Physics, Tsukuba, 305 Japan.
‖Present address: Institute for Nuclear Study, University of Tokyo, Tanashi, Tokyo 138, Japan.
¶Present address: Naruto University of Education, Naruto, Tokushima, 772 Japan.

hydrogen target and ASTERIX spectrometer [13] looked at charged π from the $\bar{p}p \to B^{\pm}\pi^{\mp}$ reaction. The result was negative in both of them. We also carried out an experiment at KEK using modularized NaI crystal to detect π^0 from the $\bar{p}p \to B^0\pi^0$ reaction, and obtained a negative result [14].

Another process one can look at is a detection of neutrons from the $\bar{p}d \to Bn$ reaction on a deuterium target. The use of a nuclear target rather than hydrogen may help the production and observation of the baryonia. In fact, Gray *et al.* who first reported a baryonium state used a deuterium target [3]. Also, detection of two narrow γ-ray lines has been reported by Adiels *et al.* in the $\bar{p}^4\mathrm{He} \to XB\gamma$ experiment, indicating two baryonium states: 1687 and 1640 [15].

The objective of the use of the $\bar{p}d \to Bn$ process in threefold: (1) As far as a liquid hydrogen target is used, the Stark mixing makes it difficult to bring in a nonzero angular momentum l to the NN system. But the ''heavy'' nucleon spectator can take out a nonzero angular momentum and thus allows us to observe states with $l \neq 0$. The centrifugal force is supposed to be essential to keep the qq and $\bar{q}\bar{q}$ or N and $\bar{N}$ apart to make the life of the baryonia long (see the discussion in Ref. [16]). (2) The baryonium states are expected to be really narrow just below the NN threshold. However, to detect the corresponding small energy γ rays in the large background stemming from abundant π^0 decays is extremely difficult, whereas, although the experiment itself is not easy, the detection of low energy neutrons is not much more difficult if the environmental background level is low enough.

Amsler *et al.* have measured the neutrons arising from the absorption of $\bar{p}$ by a liquid deuterium target at BNL [17]. They measured the time of flight of the neutrons with a resolution of ± 500 ps for a flight path of 1.4 m. They failed to observe any significant baryonium states. But we believed that this process was worth being studied again with a better statistics and a better precision for the following reasons. (1) It is desirable to obtain the charge prong information for each neutron event. This must give information on the decay of the baryonium states. Also if a baryonium decays preferentially into a specific charge prong state, its identification could improve the sensitivity of the measurement. (2) It is also interesting to measure the events with zero charge prong; namely, all associated outcoming particles are neutral. (3) It would be desirable to measure also γ ray in coincidence with the neutrons. In fact, this interesting measurement, which can shed light on the electromagnetic transition from an excited baryonium state to the ground state, has been already tried by Kalogeropoulos in their bubble chamber experiment. They counted the $\gamma \to e^+e^-$ conversion and concluded that the $\langle N_\gamma \rangle$ excess is due to baryonia [18].

Thus we undertook a measurement adding a time-of-flight neutron counter to the already existing γ-ray-detector system [1], and using a liquid deuterium target. The aim of the work is to clarify the situation of the baryonium production in the $\bar{p}d$ channel, where the experimental result is still not conclusive, by achieving a good statistics and neutron energy resolution. For this purpose, we put the neutron time-of-flight counter at about 1.2 m from the target to cover a large solid angle. Thus, given the time resolution, this experiment is sensitive in the heavy baryonium region, not far from the $\bar{p}p$ threshold. To minimize the error coming from the flight path length of the neutrons, we used all the outgoing charged particles as well as the incoming $\bar{p}$ to reconstruct the vertex point, and make the time-of-flight counter modules thin enough.

We have kept all the existing detection devices for the γ ray, so we can detect γ rays in coincidence with neutrons with a resolution as good as the results in Refs. [1], [8], and [16]. We have achieved a good energy resolution for neutrons despite the congested environment surrounding our target.

For each neutron event, the vertex charged particle topology has been reconstructed by using the chambers covering 93% of the whole solid angle.

II. EXPERIMENTAL PROCEDURE

The detector system, schematically shown in Fig. 1, consists of two parts: a time-of-flight counter which detects neutrons and the counters surrounding the target used for the detection of γ rays and charged particles. The latter consists of an NaI(Tl) counter covering 22% of 4π str, subdivided into 96 modules, and a hodoscope covering 4π geometry used to measure the multiplicity of outcoming charged particles. These counters have been used in experiments detecting γ rays and π^0 from a hydrogen target (see [1,8] for the results), and γ rays from a deuterium target (see [16,19] for the results). The detail of these counters is published in Ref. [1].

The time-of-flight counter, 72 cm high, 1.5 m long, and 9 cm thick, is made of NE110 plastic scintillator subdivided in height and in depth in 6×6 modules, each isolated optically with the aid of black paper. Each module is viewed from the ends by a couple of Hamamatsu R1828 photomultiplier tubes through adiabatic light guides used to match the 12 cm $\times 1.5$ cm scintillator section to the 2 inch photomultiplier cathode. The counter was placed with its surface parallel to the beam at a distance of 1.135 m, and with its middle line at the height of the beam. All the modules are parallel to the beam, with their center 54.2 cm downstream from the center of the target cell. The counter covers 4.07% of 4π str and, as shown later, its counting efficiency is larger than 10% for neutrons above 20 MeV even with a threshold as high as 5 MeVee (MeV electron equivalent). An anticounter to reject charged particles consisting of 8 plastic scintillators (1 cm thick) was placed vertically in front of the time-of-flight counter.

The anode signal of the photomultiplier was amplified with a timing-filter amplifier (5 ns integration, 20 ns differentiation) and then fed to the KEK type constant-fraction discriminator. The timing signal was encoded with a LeCroy 2228A and KEK type CAMAC time to digital converter (TDC). To make a residual walk correction due to the pulse height variation, the amplitude of the 11th dynode signal inverted was also recorded with a CAMAC analogue to digital converter (ADC's). The efficiency for counting neutrons of a time-of-flight counter depends critically on the discriminator threshold applied, especially for low energy neutrons. Thus for the measurement of the absolute yield, it is important to have the threshold under a precise control. During the data taking, the pulse-height threshold determined by the discriminator threshold level was kept below 1 MeVee at any

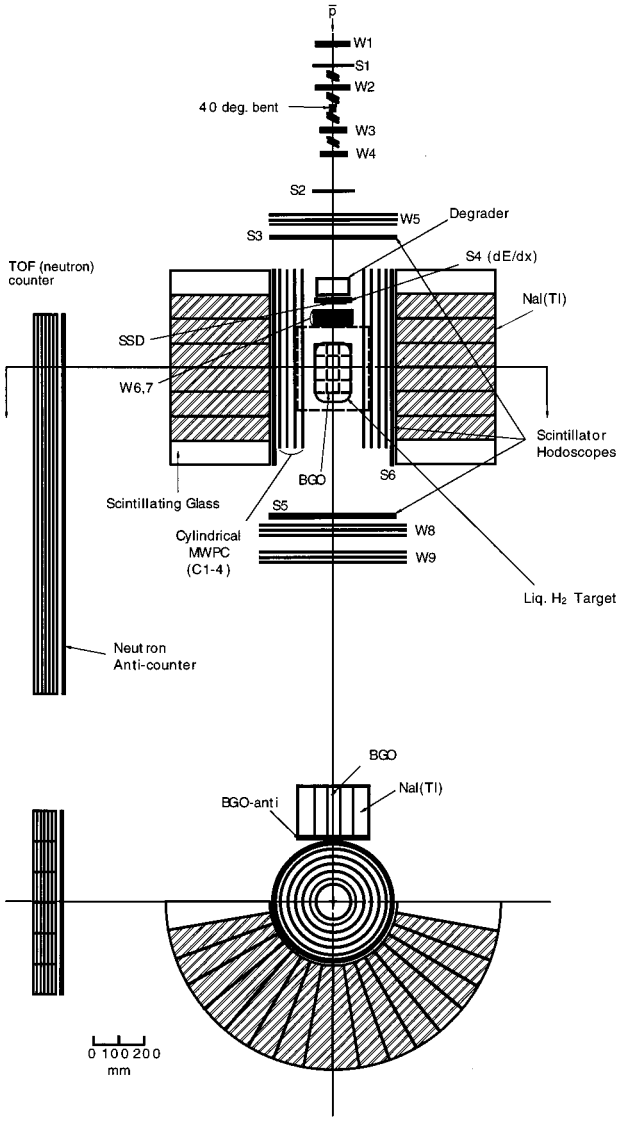

FIG. 1. Experimental setup is shown schematically. S1-S6 are plastic scintillators. W1-W9 are flat MWPC's, and C1-C4 are cylindrical MWPC's. The barrel hodoscope S6 consists of 36 scintillator slabs, each subtending 10° of azimuthal angle. The antiproton is slowed down in 8.7 g/cm^2 graphite degrader, then its energy loss is measured with S4 (1 cm thick) and 3 mm thick Si solid state detector. The time-of-flight counter, used to detect mainly neutrons, is placed at 1.135 m from the beam axis, and covers 4.07% of the whole space. 1 cm thick plastic anticounter is placed in front of the time-of-flight counter to reject charged particles.

point of the counter. Later in the data evaluation, a uniform software pulse-height threshold, independent of the position, has been applied with a light attenuation effect for each module taken into consideration. To measure the nonuniform light attenuation and the light propagation velocity in each module, a calibration measurement was carried out in which the counter was irradiated at 11 different points on each module with a 1 GeV electron beam. A typical rms timing resolution of 250 ps has been obtained for the prompt γ-ray peak (explained later) including the broadening coming from 10 cm$\times$10 cm$\times$1 cm thick start counter and from the uncertainty in the flight path length. As the prompt peak contains more low pulse height components than the signal from the neutrons, except for very slow neutrons, and the timing resolution improves with larger pulse heights, we expect this value to be the typical time resolution for the neutrons whose time of flight is less than 40 ns (above 5 MeV neutron kinetic energy). The light propagation velocity in the modules was found to be constant with in $\pm 2\%$ and was 16.1 cm/ns in average. It was no longer constant within 12 cm from each end of the module. The neutron impact point was obtained from the difference in timing in the signals from both ends. Thus the spatial resolution of the neutron hit point is about 1.3 cm rms horizontally (parallel to the beam) and 3.4 cm rms vertically. When the neutron signal was recorded by more than one adjacent module of the time-of-flight counter, the timing signal was taken from the module which yielded the largest signal, and the flight path was calculated up to that module, while the signal sizes of all the modules were added to obtain the pulse height.

The subdivision in depth of the counter into slabs 1.5 cm thick keeps the uncertainty in the flight path length to 0.43 cm rms in the direction perpendicular to the surface of the counter. As the pulse shape discrimination was not used, γ rays were also recorded.

Antiprotons from the K4 beam line were focused on the liquid D_2 target of 14 cm in diameter and 23 cm long. The momentum of the incident beam was 580 MeV/c with a spread of $\pm 2\%$ full width at half maximum (FWHM). The beam line has a two-stage separator and provides 510 antiprotons per 10^{12} ppp with an $e,\pi,\mu/\bar{p}$ ratio as small as about 8. The beam antiprotons are degraded in slabs of graphite, momentum-analyzed with a 1 cm plastic and a 3 mm silicon solid state dE/dx counter, tracked with multiwire proportional chambers (MWPC's), and then stopped in the target. When the multiplicity of the outcoming charged particles is higher than 1, the vertex is reconstructed from those tracks and the incoming $\bar{p}$ track. Otherwise, the information from the above-mentioned MWPC's and the signal from the solid-state detector is used to determine the vertex. The uncertainty in the vertex reconstruction is 0.9 cm rms, and the uncertainty in the flight path length is 1.0 cm rms at the closest point of the time-of-flight counter to the target.

A hit signal of the time-of-flight counter by a neutral particle combined with a signal of good $\bar{p}$ stop in the target area formed the trigger. About 2.5×10^6 events have been collected.

III. DATA EVALUATION AND RESULTS

A. Reduction

In the data evaluation procedure, only events with a well reproduced vertex point within the target volume were kept for further analysis. With the spatial resolution of the vertex reconstruction taken into account, events with a vertex point up to 1.5 cm outside the target volume were also accepted. The events with a neutral particle hitting the last 12 cm on both ends of the time-of-flight counter were rejected. As the data taking took a fairly long period of time, we have observed some drift in the TDC signals. Out of 36 modules of the time-of-flight counter, we have observed large drifts in timing in two modules and have discarded the events involving those modules. Also, for some period of time, we have experienced a large drift in TDC output in all the modules;

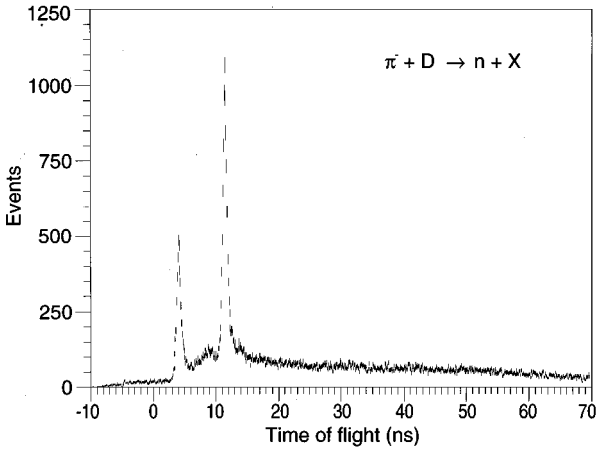

FIG. 2. The time-of-flight spectrum for the threshold of 1 MeVee obtained with the incident π^- beam. The flight path-length correction is done (see text). The prompt peak appears at 4 ns, while a large peak, due to the 68 MeV neutron from the $\pi^- d \rightarrow nn$ reaction, appears at about 11.4 ns. The peak due to the 8.86 MeV neutrons from $\pi^- p \rightarrow \gamma n$ reaction on the hydrogen contamination in the deuterium target, which should appear at 29.3 ns, is not visible.

thus we discarded the data from those runs (24 out of 210). This was partially due to the instability of the air conditioning system in the counting house. Also in 5 modules we have seen a large drift in 94 runs out of 186, and the corresponding data were discarded. As the result, about 78% of the raw data (1.98×10^6 events) have been kept for further analysis.

By knowing the vertex and the impact point of the neutral particle on the time-of-flight counter, its flight path length was calculated, which spreads between 114 cm and 135 cm. The time of flight for each particle was multiplied by the ratio of 1.2 m to the actual flight path length. We have decided to make use of these flight-path-length-corrected time-of-flight spectra to search for narrow resonances by fitting. Alternatives would be to do the fitting on the neutron momentum or energy, or on the missing-mass spectra. The advantage of our method is that the resolution is almost constant in terms of the time-of-flight, and also the deduced physical quantities about the neutrons like their momenta, etc., in the alternative methods have no meaning if the analyzed event is not due to a neutron, but a delayed γ contamination.

A huge peak at 4.0 ns ($\beta=1$) was observed, which is due to the prompt γ rays originating from the decay of π^0's produced in the annihilation of the antiprotons. Charged pions are also produced in the annihilation process, and if they interact with any material, they can emit γ rays or neutrons. These γ rays are delayed in average by Δ, which is the time necessary for those charged pions to stop. When a π^- stops in the target and is absorbed by a deuteron, two neutrons are emitted back-to-back with an energy of 68 MeV. This must produce a monoenergetic peak at 11 ns in the time-of-flight spectrum. No other neutrons except for the ones coming from the two-body decay of the $\overline{pd}$ system into Bn or Mn (M is a meson) are expected to exhibit a narrow peak in the time-of-flight spectrum in the region of interest (5 to 35 ns). To check the position of the 68 MeV neutron peak, we have taken data with an incident 160 MeV/c π^-

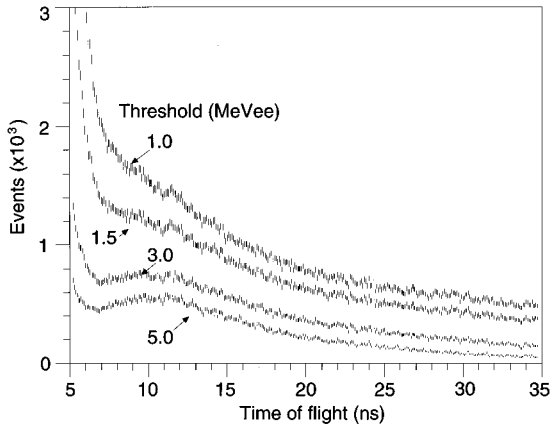

FIG. 3. Time-of-flight spectra from the $\overline{pd}$ reaction for the range of 5 to 35 ns. Different thresholds (1.0, 1.5, 3.0, 5.0 MeVee) are applied to examine the neutron components in the spectrum (see text).

beam on the same target. After being degraded, these pions stop in the target and emit either prompt γ rays associated with neutrons stemming from radiative capture by the deuteron (the contribution from the $\pi^- d \rightarrow \pi^0 nn$ process is very small), or two neutrons emitted in opposite directions with an energy of 68 MeV. The result is shown in Fig. 2. As the times of flight between the start counter and the vertex are different for the incident $\overline{p}$ and for the incident π^-, we cannot use the position of the neutron peak for the absolute calibration, but its timing with respect to the prompt γ-ray peak must be the same also in the $\overline{p}$ data. As the distance between the two peaks in Fig. 2 turns out to be 7.4 ns, we expect the peak in our data corresponding to that background monoenergetic neutron to appear at about 11.4 ns $+\Delta$.

Figure 3 shows the time-of-flight spectra of the neutron candidates in the $\overline{pd}$ reaction for the range of 5 to 35 ns with different thresholds applied. In Fig. 4 we show the neutron detection efficiency of the time-of-flight counter calculated with a Monte Carlo program [20]. By comparing Figs. 3 and 4, one notices that (1) although the efficiency does not change much between 5 and 10 ns with these different thresholds, the yield changes to a large extent. This indicates

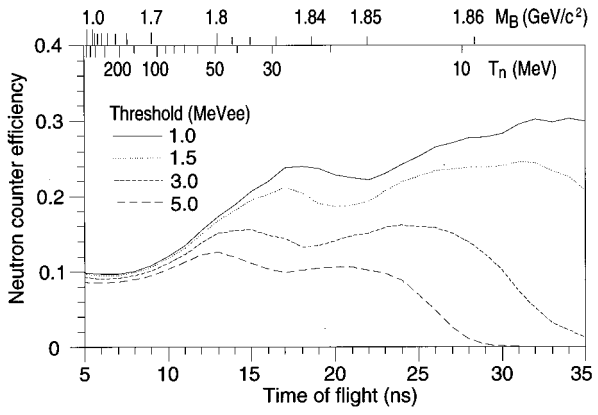

FIG. 4. Neutron detection efficiency of the time-of-flight counter. The efficiencies are calculated with a Monte Carlo program for different thresholds (1.0, 1.5, 3.0, 5.0 MeVee).

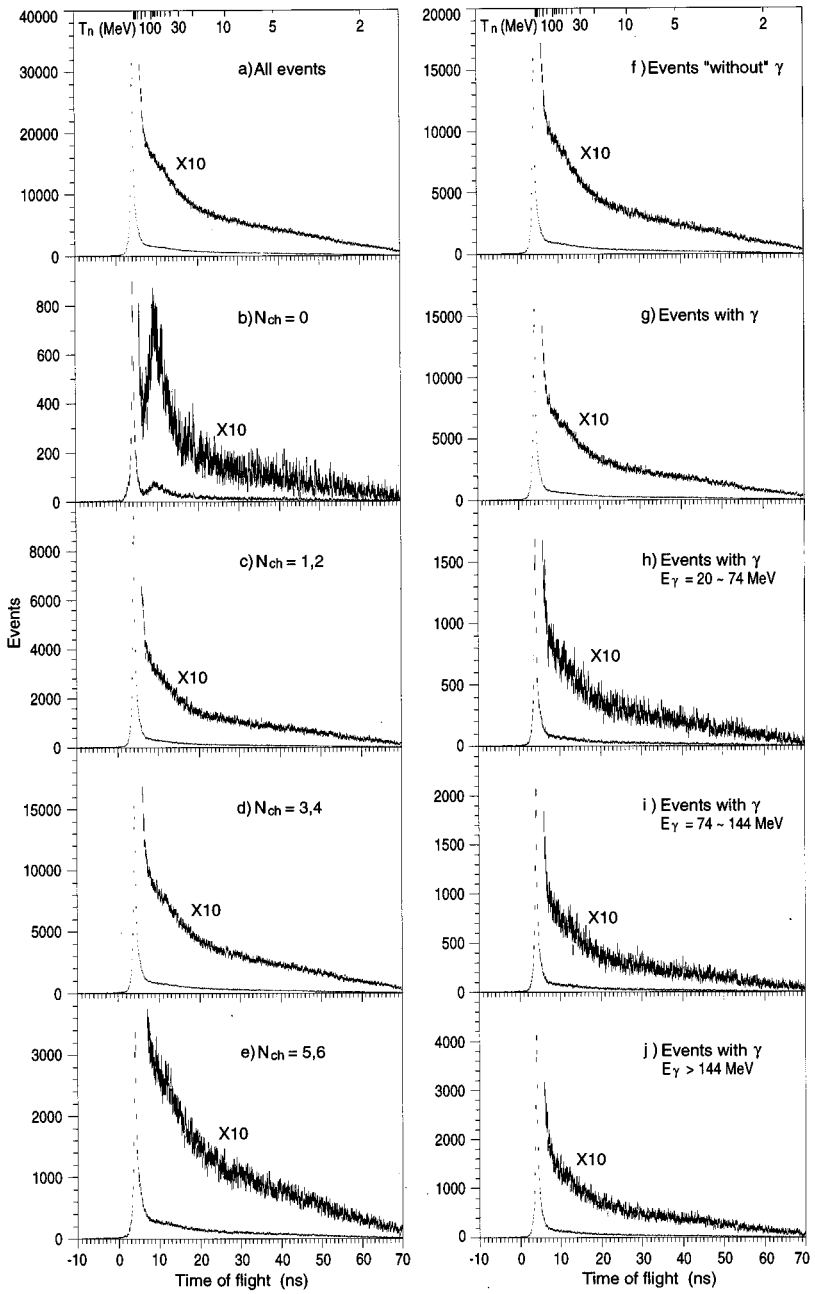

FIG. 5. Time-of-flight spectra for the $\overline{pd}$ reaction are shown for (a) all events, (b) events with multiplicity of the outcoming charged particles ($N_{\rm ch}$)=0, (c) $N_{\rm ch}$=1 or 2, (d) $N_{\rm ch}$=3 or 4, (e) $N_{\rm ch}$=5 or 6, (f) events with ''no γ in coincidence'' (see text), respectively. Spectra (g)–(j) are for events with γ in coincidence where (g) all γ, (h) E_γ=20−74 MeV, (i) E_γ=74−144 MeV, (j) E_γ>144 MeV, respectively. All the spectra shown are for the threshold of 1 MeVee.

that in the time-of-flight range between 5 and 10 ns, a fairly large amount of delayed γ-ray events, or indirect neutrons, are recorded. Here the indirect neutron means a neutron originating from the absorption of a particle like a pion the surroundings of the target. We will discuss this more extensively later. (2) In the middle time-of-flight range from 15 to 25 ns, the ratio of the efficiencies is almost equal to that of the yields with different thresholds. (3) At a large time of flight, the yield with a 5 MeVee threshold is assumed to be zero according to the efficiency curve. In fact, the yield is small, but there is still some remaining component. The remaining component, however, is not due to the room background neutron. The background neutron level is very low, which can be seen in the time-of-flight range preceding the prompt γ-ray peak in the figures shown later.

The time-of-flight spectra for all events, for events with multiplicity of the outcoming charged particles ($N_{\rm ch}$) 0, 1 or 2, 3 or 4, and 5 or 6 are shown in Figs. 5(a)–5(e), respectively. All the spectra shown in Fig. 5 are for the software threshold of 1 MeVee. A fractional binning method is used in the spectra throughout this paper in order to make the fitting easier. This method is explained in the Appendix. In the spectrum showing the all events [Fig. 5(a)], one notices a peak at 4 ns, which is mainly due to the prompt γ rays. The peak shows a tail on the slower side which is due to the delayed γ rays. One also notices a shoulder starting from about 5 ns. That is where the neutron enhancement starts. The neutrons originating from the $\overline{pd}\rightarrow Mn$ reaction, where M is a known light meson, should fall into this part. ($M=\pi^0$ at 5.01 ns, $M=\rho^0$ at 5.23 ns, $M=\omega$ at 5.24 ns, etc.)

Among the next four spectra in Figs. 5(b)–5(e), the spectrum for events with charged particle multiplicity zero [Fig. 5(b)], namely all neutral events, attracts our special attention for the following reason: As explained later, this is the only

channel where the contribution of the indirect neutrons is absent. The neutron time-of-flight spectral shape reflects well the momentum distribution of the spectator neutron in the case where the $(\overline{pp})$ system decays into only neutral pions. In fact, the shape of the distribution is quite different from other channels; the events filling the valley between the prompt peak and the neutron enhancement in other spectra are missing.

B. Narrow peaks in the time-of-flight spectra

A search for narrow peaks in the spectrum has been tried in the time-of-flight range of 5 to 35 ns. This corresponds to the neutron energy of 630 MeV to 6 MeV, or the baryonium mass of 0 to 1872 MeV/c^2 if a direct two-body production is assumed. A fit is carried out to the data with narrow peaks in Gaussian shape plus background using the CERN library MINUIT program. The background consists of a fifth degree polynomial and a Gaussian tail which is necessary to describe the rapid fall in the small time-of-flight region. Thus the background comprises 9 parameters. In this fit and in most of the fits described later, this background reduces the χ^2 per degree of freedom to almost 1. The Gaussian distribution used to describe narrow peaks is parametrized with its center position, width (rms), and area. The variance of the converged value of each parameter is calculated from the error given by MINUIT which increases χ^2 by unity. The starting values of the parameters describing peaks are chosen from the visual inspection of the data. If the introduction of a new peak does not reduce χ^2 by more than 3, that candidate was discarded.

The result of the fit is shown in Fig. 6. In the first figure, 6(a), which shows the result of a fit for the all events, the only peak which has a large statistical significance is the one at 11.9 ns, with a significance of 5.7σ. This must be the peak corresponding to the 68 MeV background neutrons mentioned earlier. We discuss this peak more extensively later.

Three other peaks observed, all with small statistical significances, are at 9.6, 14.1, and 29.4 ns with significances of 2.2σ, 3.0σ, and 1.9σ, respectively. The result of the fit is summarized in Table I. As our instrumental resolution is estimated to be about 250 ps, we put a constraint on the width such that it be larger than 250 ps. The χ^2 for 301 experimental points changed from 353.1 without any narrow peak (degree of freedom is 292) to 285.9 with 4 peaks (degree of freedom is 280).

The position of the 29.4 ns peak (corresponding to the neutron energy of 8.82 MeV) is not far from the monoenergetic neutron from the $\pi^- p \to \gamma n$ reaction (8.86 MeV) which could take place on a contaminating hydrogen in the deuterium target. We can, however, show that the contribution of this reaction to our neutron spectrum is small in the following way: The rate of the reaction $\pi^- p \to \gamma n$ is about 0.25/stopped π^-, whereas the rate of the $\pi^- d \to nn$ process on the deuterium target is nearly 1 neutron/stopped π^-. Therefore we should count 2 neutrons/stopped π^-, and in reality, we observe 13.8×10^{-3} neutrons/stopped $\overline{p}$ in our data. The hydrogen contamination in the deuterium target is estimated to about 0.9% in mol [16]. Thus the yield of neutrons from the reaction $\pi^- p \to \gamma n$ is estimated to be less than 1.5×10^{-5}/stopped $\overline{p}$, or 3 events. Thus the 29.4 ns peak, which has a yield of $(0.876\pm0.401)\times10^{-3}$/stopped $\overline{p}$ (132.2 ± 60.6 events), is not due to this background process. In fact, this can be confirmed from the neutron spectrum from the $\pi^- d$ reaction in Fig. 2. The enhancement near 29.3 ns, if there is any, is at most 170 times smaller than the $\pi^- d \to nn$ peak.

The same fit has been carried out on the spectra for different charge multiplicities $N_{\rm ch}$, and the results are listed also in Table I.

The peak at 11 ns seems to be weakly populated in the $N_{\rm ch}=0$ channel [Fig. 6(b)]. Its statistical significance, however, is small and its width is much smaller than the instrumental resolution. It should be noted that in the γ-ray spectrum from the $\overline{p}+D_2$ reaction, the 125 MeV peak due to the Panovsky γ from the $\pi^- d \to \gamma nn$ reaction was missing in $N_{\rm ch}=0$ and 1 or 2 channel, but was clearly seen in $N_{\rm ch}\geq3$ channels [1]. We also fail to see the 11 ns neutron peak in $N_{\rm ch}=1$ or 2 channel. The population of the 11 ns peak is large in $N_{\rm ch}=3$ or 4 channel, weaker in $N_{\rm ch}=5$ or 6 channel. This agrees well with the result of the γ-ray data [16] where the ratio of the yields $\Upsilon(N_{\rm ch})$ of the 125 MeV peak for different charge multiplicities $N_{\rm ch}$ is

$$\Upsilon(0):\Upsilon(1,2):\Upsilon(3,4):\Upsilon(5,6)=0:0:2.18:0.47.$$

Thus the dependence of our yield of the 11 ns peak on the charge multiplicity is similar to that of the γ rays given in Ref. [16]. This fact supports the assignment of the peak at about 11 ns to be due to the monoenergetic neutrons coming from the absorption of π^- in the target deuterium ($\pi^- d \to nn$), produced in the $\overline{p}$ annihilation. This peak, however, must appear at 11.08 ns, whereas in our fit, the position of the corresponding peak is 11.85 ± 0.11 ns (width: 0.54 ± 0.11 ns). The 0.77 ns shift is noticeable taken the resolution of 250 ps of the time-of-flight counter into consideration. To account for the shift, we estimated Δ, the flight time of the absorbed π^- in the target deuterium, by using a Monte Carlo method. The shift is about 330 ps with a peak broadening from 250 ps to 390 ps; therefore, it explains only a part of the discrepancy. We have thought of the possibility of the contribution of the $\pi^- d \to \gamma nn$ process. But this yield is only one third of the $\pi^- d \to nn$ process, and also the energy of the γ ray is known to peak very near its high limit. Angelopoulos *et al.* [10] also observed that the timing of the γ ray from the $\pi^- p \to \gamma n$ process observed in the $\overline{p}$H reaction is delayed by 800 ps with respect to the direct γ ray from the annihilation. They state that the delay is due to Δ, the flight time needed for the π^-. We ran our Monte Carlo code under their target condition, but the result was that the flight time in their case seems even smaller than in our case. It should be also noted that as mentioned earlier, the distance between the prompt peak and the peak due to the $\pi^- d \to nn$ process was 7.4 ns in the calibration run using a stopped π^- beam (see Fig. 2). This value again seems to be a little larger than the predicted value of 7.08 ns (11.08–4.0). In this case, the γ ray should come mainly from the $\pi^- d \to nn\gamma$ process; thus there is no contribution of the time needed for the π^- to stop. Therefore, in this case also we observe a discrepancy, though not as large as in the case of the $\overline{p}$ data.

The peak at 18 ns with a relatively large significance,

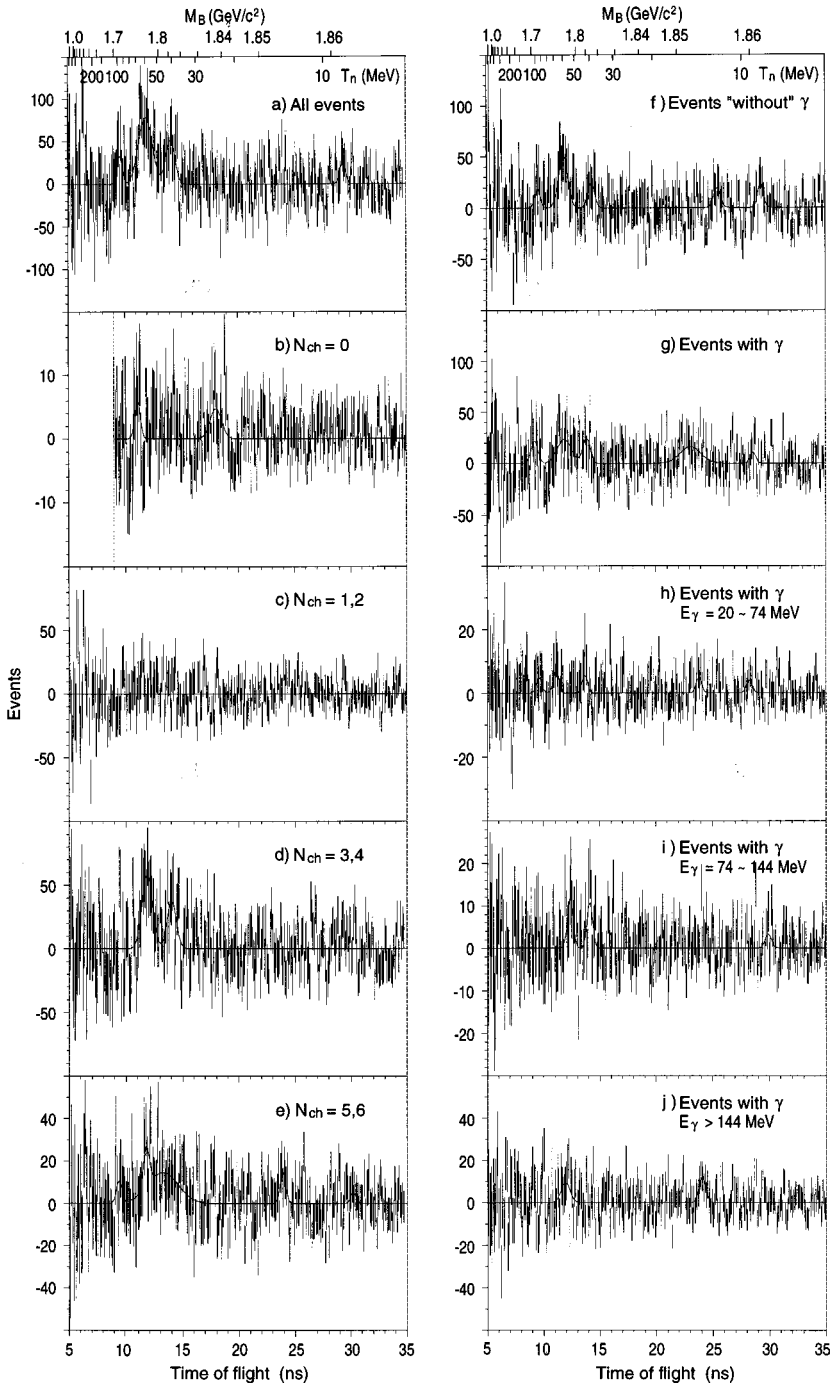

FIG. 6. The results of the fit are shown for (a) all events, (b) events with multiplicity of the outcoming charged particles (N_{ch})=0, (c) N_{ch}=1 or 2, (d) N_{ch}=3 or 4, (e) N_{ch}=5 or 6, (f) events with ''no γ in coincidence'' (see text), respectively. Spectra (g)–(j) are for events with γ in coincidence where (g) all γ, (h) E_γ=20−74 MeV, (i) E_γ=74−144 MeV, (j) E_γ>144 MeV, respectively.

although broad, was observed only in $N_{ch}=0$ channel. In $N_{ch}=5$, 6 channel, enhancements with rather small statistical significances were observed at 9.42, 23.89, and 30.19 ns. However, they are not seen in other charge multiplicity channels.

In case the emission of a neutron is associated with the emission of γ rays, we have recorded their energies. About 28% of the events are associated with at least one γ, detected by the γ-ray counter which covers 22% of the whole space. Figures 5(f) through 5(j) show the events without γ, with γ, with a low energy γ, with a medium energy γ, and with a high energy γ, respectively. Here the low, medium, and high energy means 20 to 74 MeV (minimum energy of the γ from the $\pi^- d \rightarrow \gamma nn$ process), 74 to 144 MeV (maximum), and above. When more than one γ ray are emitted, the most energetic one was used for the event classification. Here, the events ''without γ'' only mean that we have not detected γ rays with our NaI(Tl) counter which covers 22% of 4π solid angle in coincidence with those events. The results of the fit on these spectra are shown in Figs. 6(f) through 6(j). The enhancements which have been observed only in $N_{ch}=5$ or 6, namely 9.42, 23.89, 30.19 ns are also observed a little more abundantly in the events without γ at 9.58, 25.52, 29.31 ns. But they are also seen in the events with γ, although less clearly. The peak at 8 ns was seen only in the events in coincidence with low energy γ, although the significance is very small.

The results of the fit are also summarized in Table I, and

TABLE I. The results of the fit. As explained in the text, fit has been performed on the time-of-flight spectra for all events, events with multiplicity of the outcoming charged particles (N_{ch})=0, N_{ch}=1 or 2, N_{ch}=3 or 4, N_{ch}=5 or 6, events with ''no γ in coincidence'' (see text), events with γ in coincidence, in coincidence with low energy (E_γ=20−74 MeV) γ, in coincidence with medium energy (E_γ=74−144 MeV) γ, in coincidence with high energy (E_γ>144 MeV) γ. Several peaks have been observed in each spectrum except for the one for N_{ch}=1 or 2 channel, which was almost structureless. Peaks observed at approximately the same position are listed in the same row. For each peak, the time-of-flight position, the efficiency of the counter, number of events involved in the peak, reduced yield of neutrons (unit: 10^{-3}/stopped $\overline{p}$), statistical significance (in the unit of standard deviation), and width of the peak are indicated. The width of 0.25 ns means that MINUIT gave the minimum χ^2-value at the lower limit of 250 ps for the width parameter (see text). Also in the bottom, the χ^2 value, the degree of freedom, and χ^2 per degree of freedom are indicated.

	Spectrum	All	N_{ch}=0	N_{ch}=1,2	N_{ch}=3,4	N_{ch}=5,6	Without γ	With γ	w/low $E\gamma$	w/med $E\gamma$	w/high $E\gamma$
	Position (ns)								8.07±0.24		
	Efficiency								0.102		
8 ns	Number of events								41.0±25.9		
peak	Yield (10^{-3})								0.764±0.483		
	Statis. significance								1.58		
	Width (ns)								0.28±0.12		
	Position (ns)	9.55±0.15				9.42±0.23	9.58±0.012	9.21±0.20	9.60±0.16		
	Efficiency	0.113				0.111	0.113	0.109	0.113		
10 ns	Number of events	218.6±97.7				48.4±41.3	169.3±74.1	80.3±64.2	36.0±21.5		
peak	Yield (10^{-3})	3.674±1.642				0.824±0.703	2.84±1.24	1.39±1.11	0.602±0.359		
	Statis. significance	2.24				1.17	2.29	1.25	1.67		
	Width (ns)	0.25				0.25	0.25	0.25	0.25		
	Position(ns)	11.85±0.11	11.07±0.09		11.87±0.09	11.74±0.15	11.84±0.10	11.90±0.29	11.10±0.13	12.36±0.09	11.94±0.22
	Efficiency	0.151	0.136		0.151	0.148	0.150	0.152	0.136	0.161	0.153
11 ns	Number of events	997.0±170.1	53.75±18.94		653.1±112.6	134.8±73.8	609.4±123.4	349.1±110.3	49.4±21.0	71.7±20.7	87.8±41.4
peak	Yield (10^{-3})	12.50±2.14	0.749±0.264		8.20±1.41	1.72±0.943	7.70±1.56	4.35±1.38	0.688±0.293	0.844±0.244	1.086±0.513
	Statis. significance	5.86	2.84		5.80	1.83	4.94	3.17	2.34	3.47	2.12
	Width (ns)	0.54±0.11	0.25		0.45±0.09	0.28±0.12	0.45±0.11	0.62±0.23	0.25	0.25	0.37±0.25
	Position (ns)	14.09±0.13			14.04±0.12	13.49±0.46	14.34±0.16	13.86±0.17	13.65±0.14	14.08±0.09	
	Efficiency	0.195			0.194	0.184	0.200	0.191	0.187	0.195	
14 ns	Number of events	332.5±111.8			361.3±101.3	439.0±129.3	182.4±75.9	189.9±80.7	36.3±19.4	66.9±19.9	
peak	Yield (10^{-3})	3.23±1.09			3.53±0.988	4.52±1.33	1.73±0.721	1.88±0.801	0.368±0.197	0.650±0.193	
	Statis. significance	2.97			3.57	3.40	2.40	2.35	1.87	3.36	
	Width (ns)	0.32±0.10			0.39±0.14	1.32±0.37	0.30±0.10	0.32±0.15	0.25	0.25	
	Position(ns)		18.10±0.18								
	Efficiency		0.231								
18 ns	Number of events		72.6±20.3								
peak	Yield (10^{-3})		0.596±0.167								
	Statis. significance		3.58								
	Width (ns)		0.54±0.12								
	Position(ns)					23.89±0.10	25.52±0.14	23.16±0.29	23.83±0.11		24.05±0.10
	Efficiency					0.24	0.255	0.235	0.240		0.241
25 ns	Number of events					75.6±27.9	192.5±65.6	356.3±96.4	32.0±14.6		87.2±24.7
peak	Yield (10^{-3})					0.597±0.220	1.43±0.489	2.87±0.777	0.253±0.115		0.685±0.194
	Statis. significance					2.71	2.94	3.70	2.19		3.54
	Width (ns)					0.25	0.34±0.12	0.90±0.21	0.25		0.29±0.08
	Position(ns)	29.37±0.11				30.19±0.27	29.31±0.09	28.59±0.15	28.23±0.14	29.90±0.26	
	Efficiency	0.286				0.290	0.286	0.282	0.279	0.289	
30 ns	Number of events	132.2±60.6				26.82±25.70	151.0±43.5	48.9±39.1	23.3±14.4	22.7±15.2	
peak	Yield (10^{-3})	0.876±0.401				0.175±0.168	1.00±0.288	0.329±0.263	0.158±0.0978	0.149±0.0998	
	Statis. significance	2.18				1.04	3.47	1.25	1.62	1.50	
	Width (ns)	0.25				0.25	0.25	0.25	0.25	0.29±0.13	
	χ^2	255.9	185.4	314.5	292	275.3	257.6	311.3	270.2	234.2	296.8
	deg. of freedom	281–18	211–11	301–9	301–15	301–18	301–21	301–18	301–18	301–21	301–15
	χ^2/deg. of freedom	0.973	0.927	1.077	1.021	0.973	0.92	1.1	0.955	0.836	1.04

TABLE II. Characteristics of the observed ''levels'' are summarized. The position, statistical significance, number of events in the peak, efficiency of the counter, yield of neutrons/stopped $\bar{p}$, peak width, corresponding neutron energy, mass, and the width of the level are listed. When the same peak is observed in spectra of events in different categories in Table I, the parameters for each level are taken from the fit of the spectrum which gives the largest statistical significance.

Time of flight (ns)	Statistical significance	Number of events	N counter efficiency	Yield (10^{-3})	Width (ns)	E_n (MeV)	Mass (MeV/c^2)	Width (MeV/c^2)	Comment
8.07±0.24	1.58	41.0±25.9	0.102	0.76±0.48	0.28±0.12	142.2±10.5	1647.0±17.9	20.9±9.0	Seen only with low energy γ.
9.55±0.15	2.24	218.6±97.7	0.113	3.67±1.64	0.25	95.13±3.5	1725.6±5.6	9.8	Seen with N_{ch}=5,6. Not seen with medium or high energy γ.
11.85±0.11	5.86	997.0±170.1	0.137[a]	13.8	0.54±0.11	58.6±1.2	(1784.2±1.9)	(9.2±1.9)	Peak due to neutron back-to-back emission from the $\pi^- d \to nn$ reaction
14.04±0.12	3.57	361.3±101.3	0.194	3.53±0.99	0.39±0.14	40.6±0.7	1812.3±1.2	3.7±1.3	Seen with N_{ch}=3,4 and N_{ch}=5,6. Also with medium energy γ.
18.10±0.18	3.58	72.63±20.3	0.231	0.60±0.17	0.54±0.12	24.0±0.4	1838.0±0.7	2.2±0.5	Seen only with N_{ch}=0.
23.16±0.29	3.70	356.3±96.4	0.235	2.87±0.78	0.90±0.21	14.33±0.4	1852.7±0.6	1.8±0.4	Seen with N_{ch}=5,6. Stronger in events with γ than in without.
29.31±0.09	3.47	151.0±43.5	0.286	1.00±0.29	0.25	8.87±0.05	1860.96±0.09	0.40	Seen with N_{ch}=5,6. Stronger in events without γ.

[a]To calculate the yield for the 11.85 ns peak, the efficiency for 68 MeV neutron energy was used rather than the efficiency for the peak position in the time-of-flight spectra.

the information relative to each ''level'' is summarized in Table II.

From the known time-of-flight resolution and the statistics, the 4σ upper limits of the yield of neutrons per stopped $\bar{p}$ leading to narrow states (baryonia) are calculated, and shown in Fig. 7, together with the yield for the observed peaks. The formula (1) explained in the next chapter was used to calculate the yield per stopped $\bar{p}$, in which the time-of-flight counter efficiency for the neutron detection was evaluated at the neutron kinetic energy calculated from its time-of-flight. The upper limit for the yield is 5×10^{-3} for baryonia with mass $M_B > 1800$ MeV/c^2, and 1.0×10^{-2} for 1800 MeV/$c^2 > M_B > 1700$ MeV/c^2 per stopped $\bar{p}$. If the baryonia decay preferentially into specific N_{ch} channels, then the upper limit is smaller as shown in Fig. 7.

In the region near the $\pi^- d \to nn$ peak (68 MeV neutron energy, 1750 MeV/c^2 M_B), the 4σ upper limit for the yield is 7.2×10^{-3} per stopped $\bar{p}$. This value is consistent with the fact that the peak due to the $\pi^- d \to nn$ process, whose yield is estimated to be 13.8×10^{-3} neutrons per stopped $\bar{p}$, shows up as a 5.9σ. The above result can be compared with the result by Amsler *et al.* obtained in an experiment at BNL [17]. In the same region, their 4σ upper limit was about 2.8×10^{-3}, actually smaller than the present value. This value, however, is difficult to understand, since (1) the statistics of the present experiment are more than 2 times better, and the time-of-flight resolution is 2.7 times better than that of Ref. [17], and that (2) the peak corresponding to the $\pi^- d \to nn$ process is hardly visible in the spectrum of Ref. [17], while that yield is estimated to be about 1×10^{-2} per stopped $\bar{p}$ or larger in their experimental condition, therefore the peak would have shown up as a 14σ peak with their 4σ upper limit.

C. Various rates

Assuming that the 11 ns peak is due to the $\pi^- d \to nn$ reaction, we used the number of events included in this peak to evaluate the yield of different peaks.

In our previous paper [16], the yield of γ rays from the radiative capture process $\pi^- d \to \gamma nn$ has been determined to be 2.3×10^{-3} per $\bar{p}$ stop in our experimental condition. On the other hand, it is known that the ratio of the rates $R(\pi^- d \to nn)/R(\pi^- d \to \gamma nn)$ is very close to 3 [21]. This means our peak at 11.9 ns in Fig. 6(a), which contains 997.0±170.1 events, corresponds to a yield of $2\times6.9\times10^{-3}$ neutrons per stopped $\bar{p}$. As the efficiency of the time-of-flight counter for 68 MeV neutrons is 0.137, the yield Υ per stopped $\bar{p}$ of a state corresponding to a peak containing S events can be calculated as

$$\Upsilon = 0.137\times1.38\times10^{-2} S/[997\varepsilon(t)] = 1.90\times10^{-6} S/\varepsilon(t), \quad (1)$$

where $\varepsilon(t)$ is the efficiency of the time-of-flight counter at time-of-flight t. On the other hand, the yield per stopped $\bar{p}$ of the 68 MeV peak should be expressed as:

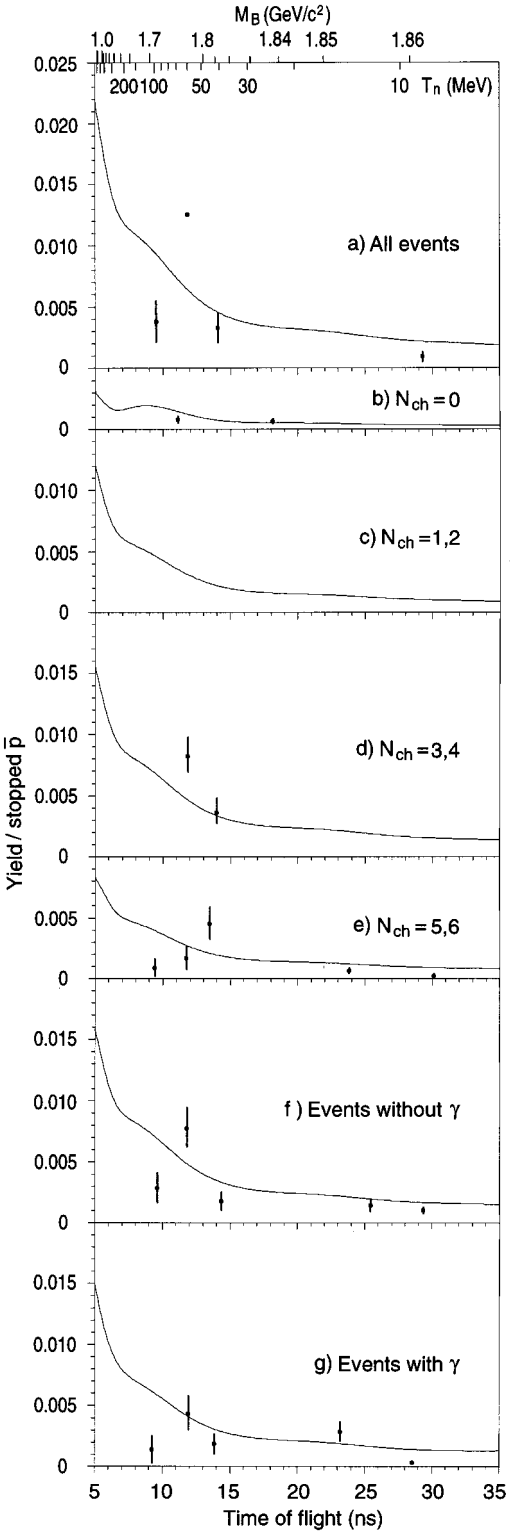

FIG. 7. From the known time-of-flight resolution and the statistics, the 4σ upper limits of the yield of neutrons per stopped $\overline{p}$ leading to narrow states (baryonia) are calculated. The results are shown for all events, events with multiplicity of the outcoming charged particles ($N_{\rm ch}$)$=0$, $N_{\rm ch}=1$ or 2, $N_{\rm ch}=3$ or 4, $N_{\rm ch}=5$ or 6, events with ''no γ in coincidence'' (see text), and for events in coincidence with γ, respectively. The yields for the observed peaks are also shown.

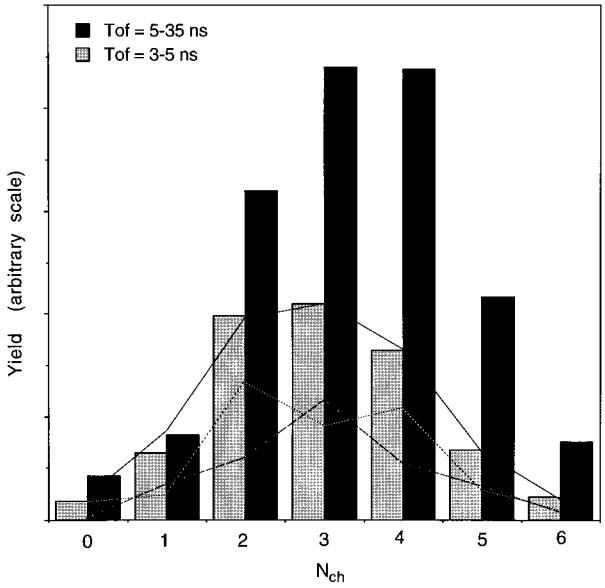

FIG. 8. The dependence of the integrated number of events on the charge multiplicity of the outcoming particles $N_{\rm ch}$. The grey data bars are for events in the prompt peak (time of flight $=3$–5 ns) whereas black bars are for neutron components (time of flight $=$ 5–35 ns). The solid line represents the γ-ray yield from the $\overline{pd}\to X\gamma$ reaction, taken from Ref. [16]. In Ref. [16], the γ-ray yield is decomposed into the contribution from $\overline{pp}$ annihilation (shown with dotted line) and $\overline{pn}$ annihilation (dashed line), using the result from Ref. [14] on the $\overline{pp}\to X\gamma$ reaction. The dotted line shows a zigzag trend indicating that the yield for odd $N_{\rm ch}$ is relatively small, whereas the neutron (black bars) distribution is rather smooth, and the center is shifted to a larger $N_{\rm ch}$ compared to the γ-ray-yield distribution.

$$\Upsilon_{68\ \mathrm{MeV}n}=2\times N_{\overline{p}\mathrm{stop}}\times\frac{\Delta\Omega}{4\pi}\times\varepsilon(t\ \text{ for }\ E_n=68\ \mathrm{MeV})$$
$$\times\varepsilon_{\mathrm{reconst}}\times\eta(\overline{p}\pi^-d\to nn), \tag{2}$$

where $\Delta\Omega$, $\varepsilon_{\rm reconst}$, and η are the solid angle covered with the time-of-flight counter, the event reconstruction efficiency, and the nn rate (6.9×10^{-3}/stopped $\overline{p}$), respectively. Then $\varepsilon_{\rm reconst}\times N_{\overline{p}\rm stop}$ becomes 1.17×10^7 which turns out to be consistent with the total number of stopped $\overline{p}$ estimated in the $\overline{pd}\to X\gamma$ reaction [16]. The yields shown in Table II have been calculated in this manner.

1. The prompt peak

In the time-of-flight spectrum for all events [Fig. 5(a)] the number of events between 3 and 5 ns is about 2.6×10^5. The $N_{\rm ch}$ distribution of those events shown in Fig. 8 is very close to the $N_{\rm ch}$ distribution of the γ-ray events in the $\overline{pd}$ annihilation [16]. Thus we infer that these events are mainly due to the prompt γ rays from the π^0 decay. In fact, the number of γ rays from this decay is estimated as

$$N_\gamma=n_\gamma\times\frac{\Delta\Omega}{4\pi}\times\varepsilon_\gamma\times\varepsilon_{\mathrm{reconst}}\times N_{\overline{p}\mathrm{stop}} \tag{3}$$

where $n_\gamma=3.77$ is the average number of emitted γ rays per stopped $\overline{p}$ from the deuterium target given in the Ref. [22],

and ε_γ is the detection efficiency of 10–140 MeV γ rays by a 9 cm plastic scintillation counter, and can be roughly estimated to be 15%. By using the number $\varepsilon_{\rm reconst}\times N_{\bar{p}\,\rm stop}=1.17\times10^7$, N_γ becomes 2.7×10^5, thus the above-mentioned interference is justified.

2. Neutrons and their N_{ch} distribution

In the time-of-flight spectra, events between 6.5 and 40 ns are considered to be predominantly neutron events. This time-of-flight range corresponds to the neutron energy range of 4.7 to 252 MeV if these neutrons are produced directly from the absorption of $\bar{p}$. The number of neutrons involved in this range is 2.9×10^5, and this corresponds to a yield of 3.13 neutrons per stopped $\bar{p}$ calculated using Eq. (1). On the other hand, if we estimate the rate for the process: $\bar{p}d\rightarrow(\bar{p}\bar{p})+n_{\rm spectator}$, assuming $(\bar{p}\bar{p})/(\bar{p}n)=1.33$ (see [16]), then we obtain that the number of spectator neutrons n_n (spectator) $\approx1.33/(1+1.33)=0.57$ per stopped $\bar{p}$, which is only one fifth of the detected neutrons. The remaining neutrons should come from the absorption of stopped π^- and from the reaction of π^- in flight in the environment, mainly the NaI detectors and the iron supports, covering roughly one third of the solid angle. In fact, if we assume that $n_\gamma=3.77$ [23], and furthermore $n_\gamma\cong2n_{\pi^0}$, $n_{\pi^0}\cong n_{\pi^-}$, then the average number of π^- emitted is estimated to be about 1.9 per stopped $\bar{p}$. Anderson *et al.* [24] report that in the stopped π^- absorption, the average numbers of neutrons above 1.8 MeV emitted from C, Al, Cd, and Pb targets are 2.8 ± 0.3, 3.2 ± 0.3, 3.6 ± 0.4, and 3.5 ± 0.4, respectively. Thus in our case, as the emission of π^- as well as neutrons is isotropic, the time-of-flight counter is estimated to record about 1.2 neutrons per stopped $\bar{p}$ in the whole time-of-flight range with the threshold set to 1 MeVee. Neutrons originating from the reaction of the pions before stopping should also increase the number of indirect neutrons. When the neutron is a spectator, the total charge of the residual system is 0. Thus we can expect that the amount of neutrons for the channels $N_{\rm ch}=$ even is much larger than that for $N_{\rm ch}=$ odd. In fact, in the $N_{\rm ch}$ dependence of the γ-ray emission in the $\bar{p}p$ annihilation from the $\bar{p}d\rightarrow X\gamma$ reaction published in Ref. [16] (reproduced in Fig. 8), the contribution of $N_{\rm ch}=3$ is considerably small compared to the contribution of $N_{\rm ch}=2$ and 4. Our distribution given in the same figure, however, shows that the rate for $N_{\rm ch}=3$ is much larger than that for $N_{\rm ch}=2$, and is almost equal to that for $N_{\rm ch}=4$. This can be accounted for by the fact that there are many more indirect neutrons than the spectator neutrons.

It is known that the neutron emission from stopped π^- in a nuclear target is mainly through two-nucleon processes in the high-energy region, and evaporation in the low-energy region. Therefore the energy spectrum of the emitted neutron is free from fine structure [25]. Also, as the variation of the distance between the time-of-flight counter hit position and the suspected origin of the background neutrons is quite large, this should smear out any remaining fine structure in the time-of-flight spectrum of the indirect neutrons which constitute the background in our narrow-peak search. It should be noted, however, that for these indirect neutrons, the kinetic energy is different from that calculated from the observed time of flight. As the neutron-counter efficiency, and the counter acceptance to some extent, are not correct, the yield of the continuum neutrons calculated using Eq. (1) contains some error.

Further, note should be taken regarding the following.

(1) In the $N_{\rm ch}=0$ channel where all the outcoming particles are neutral, there is not contribution from the above-mentioned indirect processes. The observed neutrons consist of (a) a spectator neutron leaving a $(\bar{p}p)$ system, (b) a monochromatic neutron from the $(\pi^-,2n)$ reaction induced by the π^- from $(\bar{p}n)$ annihilation, and (c) very few neutrons from the target vessel (0.2 mm thick SUS) and supporting walls (4 mm thick aluminum), which absorb π^- from the same annihilation.

(2) In $N_{\rm ch}=1$ channel, there is no contribution of the spectator neutron, except for the miscounting of $N_{\rm ch}=2$ case. This channel must be dominated by the indirect neutrons.

Figure 8 shows the $N_{\rm ch}$ dependence of the neutron events. Note should be taken that the distribution shows a maximum between $N_{\rm ch}=3$ and 4, and that it is shifted to the larger $N_{\rm ch}$ side compared to the $N_{\rm ch}$ dependence of the γ-ray events [1] or of the prompt events mentioned in Sec. III C 1. This supports the above-mentioned assumption since larger number of pions (large $N_{\rm ch}$) should promote emission of more indirect neutrons. In addition, a large $N_{\rm ch}$ results in smaller average energy of pions which also should boost the process.

When the π^-'s are absorbed at rest by (or π^+'s interact in flight with) anything, γ rays are also emitted. Some of these γ rays are also detected by the time of flight counter. These γ rays are delayed with respect to the prompt γ ray due to the flight time of the pions. Therefore these γ rays should contribute to extend the slower-side tail of the prompt peak.

D. Spectator neutron momentum distribution

Riedberger *et al.* [26] have found a ''shoulder'' at about 400 MeV/c in the spectator proton (p_s) momentum distribution in the $\bar{p}d\rightarrow3\pi^-2\pi^+p_s$ and $\bar{p}d\rightarrow2\pi^-\pi^+p_s$ reactions.

In Fig. 9, we show the neutron momentum distribution over a wide range in the channel $N_{\rm ch}=0(\bar{p}d\rightarrow m\pi^0n_s$, $m\geqslant2)$ observed in the present experiment. This channel is the most free from the indirect neutrons. A clear sign of a shoulder at about 400 MeV/c is observed, and in fact the overall shape is rather similar to the result of Riedberger *et al.* for the protons from the above-mentioned reactions. However, in our case, the kinetic energy of the neutrons contained in the peak at $p_n<60$ MeV/c is very small; thus the counting efficiency of the time-of-flight counter for them is also very small, and the error in rate becomes large in the $p_n<60$ MeV/c range. So we cannot deduce the ratio of the height of the ''shoulder'' to that of the quasifree peak. On the contrary, we can evaluate the height of the shoulder in terms of absolute rate. It is clear that the shoulder is present; it is at about 400 MeV/c, and the dip in between is clearer than in case of Ref. [26].

In that momentum range, the neutron is no more a simple ''spectator.'' Figure 9 also draws the distribution calculated with a simple spectator model using deuteron wave functions due to Hulthén and Sugawara [27], and Hamada and Johnston with a hard-core and D-wave contribution [28].

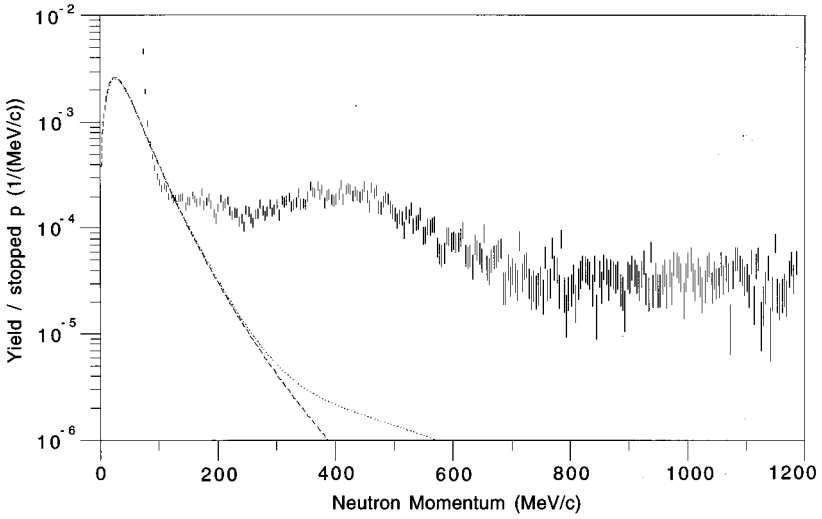

FIG. 9. Momentum distribution of the neutrons with time of flight between 5 and 50 ns for $N_{\rm ch}=0$ channel. A shoulder at about 400 MeV/c is observed. Events for very small momenta are omitted because of the inefficiency of the counter. Also shown are the momentum distribution calculated with a simple spectator model using deuteron wave functions due to Hulthén and Sugawara (dashed curve) and Hamada and Johnston (dotted curve). They are both normalized arbitrarily.

The simple spectator model is obviously not valid in the momentum range around 400 MeV/c.

Kudryavtsev and Tarasov [29] argued that an inclusion of the simple diagram with absorption of a pion (triangular diagram) allows to reproduce the shoulder observed in Ref. [26]. Their calculation includes a free parameter and also the result is now shown in terms of absolute rate.

E. γ-rays in coincidence with the neutron

We also measured γ rays in coincidence with neutrons. The γ rays in coincidence with neutrons in this reaction was observed by Kalogeropoulos *et al.* [4] and also by Amsler [30] with limited statistics.

Figure 10 shows the energy spectra of the γ rays emitted in coincidence with the neutrons whose time of flight is between 5 and 70 ns. The entries to the spectra are multiple when more than one γ ray were detected in an event. In this figure, events are also classified according to $N_{\rm ch}$. We observe the general trend that the average γ-ray energy becomes smaller with increasing $N_{\rm ch}$, as was already observed in the measurement of the γ ray from the $\overline{pd}\rightarrow X\gamma$ reaction [16]. In fact, the distributions are very similar to those which are measured in the $\overline{pd}\rightarrow X\gamma$ reaction. A small difference is observed in the small γ-ray energy region (<150 MeV), where the present (coincident) spectrum seems more suppressed. The distributions are rather smooth; we do not observe any significant structure in them. The γ-ray energy distribution measured by Amsler [30] shows a rather similar trend, although it goes only up to 300 MeV, and the statistics are limited. Compared to the present measurement, the high-energy component is smaller in their case (the ratio of the yield at 75 MeV and 300 MeV is 3:1 in the present measurement, whereas it is about 5:1 in [30]). Assuming that acceptance is corrected in both cases, we infer that their trigger condition favored large $N_{\rm ch}$. (In the present measurement, the above-mentioned ratio is 3.4:1 for $N_{\rm ch}=3$, 4, and 6:1 for $N_{\rm ch}=5,6$.)

The γ-ray energy spectra summed over $N_{\rm ch}$ are shown in Fig. 11 separately for different neutron time-of-flight ranges. The ranges are chosen so that the corresponding baryonium mass M_B is between 1.865–1.872 GeV/c^2, 1.8–1.865 GeV/c^2, 1.6$-$1.8 GeV/c^2, and 1.4$-$1.6 GeV/c^2. No clear signal of structure is observed either in these spectra.

IV. CONCLUSIONS AND SUMMARY

To search for baryonium states, a highly sensitive experiment with a good statistics has been carried out at KEK by using an antiproton beam, deuterium target, time-of-flight counter together with modularized NaI(Tl) detector to measure the neutrons from the $\overline{pd}\rightarrow Bn$ reaction and γ rays in coincidence with the neutrons. This permitted measuring the neutrons together with the coincident γ rays and obtain also the charge prong information. The neutron spectrum in the $N_{\rm ch}=0$ channel, where all outcoming particles are neutral, has been obtained for the first time.

A fit has been performed in the time-of-flight spectra to search for narrow peaks due to the formation of baryonium states. Apart from the prompt γ-ray peak at 4 ns, the only peak statistically significant is the one at 11 ns, which is assigned to the neutrons created in the $\pi^- d\rightarrow nn$ reaction where the π^- is produced in the annihilation of $\overline{p}$ and stopped in the target.

Four more peaks with a statistical significance above 3σ, and two with lower significances, were also found.

Events have been classified according to $N_{\rm ch}$ the number of outgoing charged tracks, and for each, the time of flight spectrum was studied. The spectrum for $N_{\rm ch}=0$ is particularly interesting since this shows the distribution of the spectator neutrons leaving a $(\overline{pp})$ system decaying into all neutral particles. In other channels, the spectra are contaminated with the neutrons following the absorption of π^- by the material in the environment.

The origin of the observed neutrons can be considered roughly as follows: Initially $1.17\times10^7\,\overline{p}$'s stop in the deuterium target. In 57% of the cases (6.7×10^6) a spectator neutron is emitted leaving a neutral system $(\overline{pp})$. In the rest, a spectator proton is emitted leaving a $(\overline{pn})$ negative charge system, but the low energy proton stops inside or outside the target.

The $(\overline{pp})$ or $(\overline{pn})$ system annihilates mainly into multiple pions of different charges. The π^0 decays into 2γ, and $(2-3)\times10^5$ γ rays are detected by the time-of-flight counter as the prompt peak. Most of the π^-'s leave the

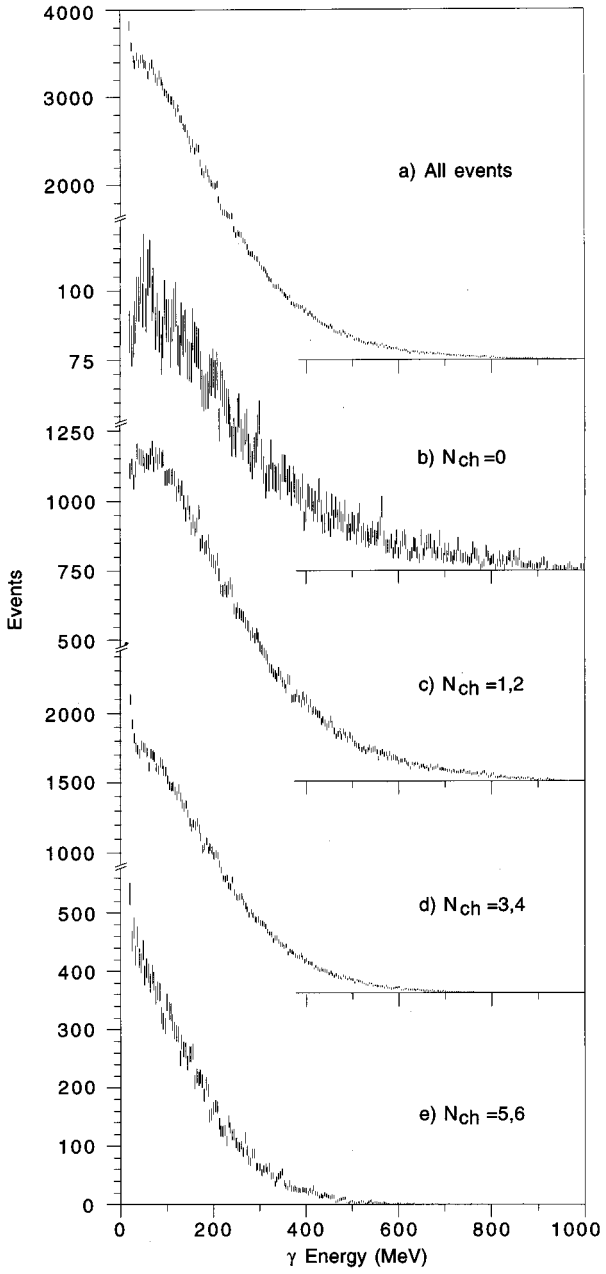

FIG. 10. Energy spreads of the γ rays associated with the neutrons whose times of flight are between 5 and 35 ns. The entries to the spectra are multiple when more than one γ rays were detected in an event. Spectra are shown for all events, events with $N_{\rm ch}=0$, $N_{\rm ch}=1$ or 2, $N_{\rm ch}=3$ or 4, and $N_{\rm ch}=5$ or 6, respectively. For γ-ray-energy resolution, see Ref. [1,14].

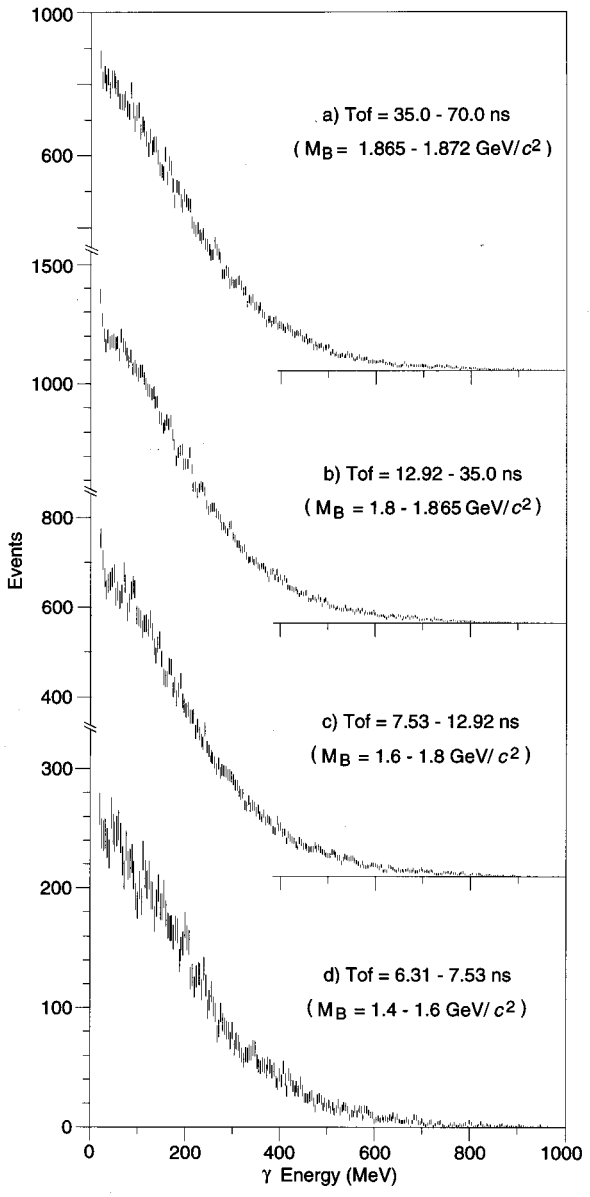

FIG. 11. Energy spectra of the γ rays associated with the neutrons in the time-of-flight range of (a) 12.92 to 35.0 ns, (b) 7.53 to 12.92 ns, and (c) 6.31 to 7.53 ns, respectively. The events are summed over $N_{\rm ch}$. The entries to the spectra are multiple when more than one γ ray were detected in an event. These neutron time of flight ranges corresponds to the ranges of baryonium mass M_B of (a) 1.8–1.872 MeV/c^2, (b) 1.6–1.8 MeV/c^2, and (c) 1.4−1.6 MeV/c^2, respectively. For γ-ray-energy resolution, see Refs. [1,14].

target and are absorbed by the environment, mainly the NaI counter. Each stop of π^- produces about 3 neutrons together with some γ rays; 3.7×10^5 neutrons are detected by the time-of-flight counter. On the other hand, a part of the π^-'s are absorbed by the deuterium in the target, and produce 68 MeV neutrons; about 1000 of them are detected by the time-of-flight counter. A part of the π^+'s interact in flight with the environment, and some of the produced neutrons are also detected by the time-of-flight counter. The contribution of K^- produced in the annihilation of $(\overline{pp})$ or $(\overline{pn})$ system (2.4%) decaying into $\pi^-\pi^0$ (21%), $\pi^0\rightarrow2\gamma$ is much smaller (estimated to be about 10^{-3}) than the γ rays from the other processes mentioned above. γ rays stem also from the π^- decays into $\mu\nu\gamma$, but the contribution is very small.

From the measured time-of-flight spectra and the known resolution, 4σ upper limits for the yield of neutrons leading to narrow baryonium states per stopped $\overline{p}$ are deduced for each $N_{\rm ch}$ channel separately as well as for all the $N_{\rm ch}$ channels added. The added yield upper limit is 5×10^{-3} for baryonia with mass $M_B>1800$ MeV/c^2, and 1.0×10^{-2} for 1800 MeV/$c^2>M_B>1700$ MeV/c^2 per stopped $\overline{p}$. If the baryonia decay preferentially into specific $N_{\rm ch}$ channels, then the upper limit for the yield is smaller, as shown in Fig. 7.

γ rays in coincidence with the neutron were also measured. The energy spectra are very similar to those obtained in the $\overline{pd} \to X\gamma$ reaction. Events are also classified according to the mass ranges of the possible baryonia. No significant structure has been observed.

ACKNOWLEDGMENTS

The authors express their deep thanks to Professor T. Nishikawa, Professor S. Ozaki, Professor H. Sugawara, Professor H. Hirabayashi, and Professor K. Nakai for supporting the present work, and to the technical staff of KEK for giving valuable help during the experiment.

APPENDIX: FRACTIONAL BINNING

In a normal binning, when an event falls between centers of two adjacent bins, the contents of the bin, whose center is closer to the event are incremented by one, and the other bin is left intact. In the fractional binning which we used here, ''one event'' is shared between the two adjacent bins. Suppose the centers of the two adjacent bins 1 and 2 are x_1 and x_2, if an event falls at x where $x_1 < x < x_2$, then the contents of bin 1 are incremented by $(x_2 - x)/(x_2 - x_1)$, whereas the contents of bin 2 by $(x - x_1)/(x_2 - x_1)$. The closer the event to bin 1, the greater the fraction bin 1 gets. This method of binning is known to reduce the statistical fluctuation of the number of events in a bin. It can be shown theoretically that the fluctuation is reduced by a factor of 0.81 when the parent distribution is flat. It can be demonstrated by numerical simulations that even when the parent distribution has a structure (like peaks), the fluctuation is reduced almost by the same amount if the bin width is narrow enough.

This effect therefore makes the fitting easier. This is not like a normal smoothing where one reprocesses already binned events. When there is an isolated peak in the parent distribution, the parameters such as the center and the width, and of course, the area of the peak, are rather well reproduced in the spectrum if the binning is not too coarse. For these reasons, we used the fractional binning to create spectra throughout this paper.

To calculate the χ^2 of a fit, terms which consist of the square of the deviation of the contents of a bin from the fitted value, divided by the square of the fluctuation of the bin content, which is usually replaced by the contents themselves, assuming a Poisson distribution, are summed over all the bins. In our case, these terms are further multiplied by $1.524 (= 1/0.81^2)$ to compensate the reduction of the fluctuation in the spectrum.

[1] M. Chiba *et al.*, Phys. Rev. D **36**, 3321 (1987).
[2] N. A. Graf *et al.*, Phys. Rev. D **44**, 1945 (1991). There is a very good compilation of the experimental results related to the baryonium search up to the date.
[3] L. Gray *et al.*, Phys. Rev. Lett. **26**, 1491 (1971).
[4] T. E. Kalogeropoulos *et al.*, Phys. Rev. Lett. **35**, 824 (1975).
[5] P. Pavlopoulos *et al.*, Phys. Lett. **72B**, 415 (1978).
[6] B. Richter *et al.*, Phys. Lett. **126B**, 284 (1983).
[7] T. Brando *et al.*, Phys. Lett. **139B**, 133 (1984).
[8] M. Chiba *et al.*, Phys. Lett. B **177**, 217 (1986).
[9] L. Adiels *et al.*, Phys. Lett. B **182**, 405 (1986).
[10] A. Angelopoulos *et al.*, Phys. Lett. B **178**, 441 (1986).
[11] R. Bertini *et al.*, Nucl. Phys. **B209**, 269 (1982).
[12] A. Angelopoulos *et al.*, Phys. Lett. **159B**, 210 (1985).
[13] S. Ahmad *et al.*, Phys. Lett. **157B**, 135 (1985).
[14] M. Chiba *et al.*, Phys. Lett. B **202**, 447 (1988).
[15] L. Adiels *et al.*, Phys. Lett. **138B**, 235 (1984).
[16] M. Chiba *et al.*, Phys. Rev. D **44**, 1933 (1991).
[17] C. Amsler *et al.*, Phys. Rev. Lett. **44**, 853 (1980).
[18] T. E. Kalogeropoulos *et al.*, Phys. Rev. Lett. **33**, 1635 (1974).
[19] M. Chiba *et al.* (unpublished).
[20] B. C. Byrd *et al.*, Nucl. Instrum. Methods Phys. Res. A **313**, 437 (1992); **313**, 457 (1992).
[21] R. MacDonald *et al.*, Phys. Rev. Lett. **38**, 746 (1977); J. W. Ryan, Phys. Rev. **130**, 1554 (1963).
[22] T. E. Kalogeropoulos *et al.*, Phys. Lett. **228B**, 424 (1983).
[23] T. E. Kalogeropoulos *et al.*, Phys. Rev. Lett. **33**, 1631 (1974).
[24] H. L. Anderson *et al.*, Phys. Rev. **133**, B392 (1964).
[25] J. Hüfner, Phys. Rep., Phys. Lett. **21**, 1 (1975).
[26] J. Riedlberger *et al.*, Phys. Rev. C **40**, 2717 (1989).
[27] L. Hulthén and M. Sugawara, *Handbuch der Physik* (Springer-Verlag, Berlin, 1957), Vol. 39, p. 1.
[28] T. Hamada and I. D. Johnston, Nucl. Phys. **34**, 382 (1962).
[29] A. E. Kudryavtsev and V. E. Tarasov, Sov. J. Nucl. Phys. **54**, 36 (1991).
[30] C. Amsler, *Advances in Nuclear Physics* (Plenum Press, New York, 1987), Vol. 18, p. 183.